Unified Model of Linear and Nonlinear Crosstalk in Multi-Core Fiber

Andrés Macho, *Student Member, IEEE*, Maria Morant, *Member, IEEE*, and Roberto Llorente, *Member, IEEE*

***Abstract*— In this paper, the theoretical unification of linear and nonlinear inter-core crosstalk (IC-XT) in step-index single-mode multi-core fiber (MCF) media is reported and validated experimentally. In order to estimate the IC-XT when operating in linear and nonlinear regimes, the coupled-mode theory (CMT) and the coupled-power theory (CPT) have been unified in both power regimes. The theoretical analysis of the CMT indicates that in coupled MCFs with reduced core-to-core distance (core pitch) the nonlinear self-coupling and cross-coupling effects should be considered when operating with high optical powers. However, considering a core pitch value higher than three times the core radius only the self-coupling effect should be taken into account for estimating the nonlinear IC-XT. Considering these results, the CPT is also extended to nonlinear regime including the dominant nonlinear coupling effect. Using both CMT and CPT, the statistical model of nonlinear IC-XT is completed with the closed-form expressions for estimating the cumulative distribution function, the probability density function and the crosstalk mean and variance as a function of the power level launched into a single-core of the MCF. The crosstalk model presented is additionally extended when multiple cores are simultaneously excited. Finally, the theoretical model is experimentally validated in a homogeneous four-core fiber considering different bending radius configurations.**

***Index Terms*— Multi-core fiber, coupled-mode theory, coupled-power theory, inter-core crosstalk.**

I. Introduction

MULTI-CORE fiber (MCF) and advanced optical modulation formats supporting space-division multiplexing (SDM) is a major focus of recent investigation in optical systems in order to overcome the capacity limit of single-core fibers [1]−[6]. The channel capacity growth is slowed down as the nonlinear Shannon limit of the single-core fiber is rapidly reached [6]. In this scenario, an attractive technology to overcome this capacity limit is SDM technology using MCF. One of the main physical impairments in SDM transmissions using MCF media is the mode coupling among cores, referred as the inter-core crosstalk (IC-XT) phenomena, which presents a stochastic nature due to the MCF random perturbations and additional birefringence fluctuations [7]−[15]. In linear regime, theoretical models using the coupled-mode theory (CMT) and the coupled-power theory (CPT) have been extensively investigated for estimating the crosstalk in coupled and uncoupled MCFs [7]−[12]. In nonlinear regime, the Manakov equations have been extended to multi-mode and multi-core fiber media modeling intra- and inter-core nonlinear effects [13], [14]. In addition, in [15] the nonlinear CMT has been recently proposed for uncoupled MCFs and the probability density function (pdf) of the nonlinear IC-XT has been reported.

Aimed to unify the crosstalk theoretical models in both power regimes for step-index MCFs considering both coupled and uncoupled cores, the nonlinear CMT should be revisited including additional mode-coupling coefficients (MCCs), the CPT should be extended to nonlinear regime from the nonlinear CMT and the statistical analysis reported in [15] should be completed with the analytical expressions of the cumulative distribution function (cdf), mean and variance of the nonlinear IC-XT. Furthermore, in bent and twisted MCFs the discrete longitudinal evolution of IC-XT can be observed at each phase-matching point where the equivalent refractive index difference between cores is zero [10], [12]. Therefore, the number of phase-matching points of the MCF is an additional parameter that can also be investigated in both power regimes.

This paper reports the theoretical estimation of the nonlinear IC-XT in MCF media in good agreement with extensive experimental measurements. The paper is structured as follows. In Section II, the nonlinear CMT is revisited to describe mode coupling in coupled and uncoupled step-index MCFs considering different core-to-core distances (core pitch) and different index mismatching values among cores. In Section III, the CPT is extended to nonlinear regime including the dominant nonlinear effect of the nonlinear CMT. In Section IV, the IC-XT statistical model is completed in nonlinear regime with the closed-form expressions of the cdf, mean, variance and number of phase-matching points of the crosstalk considering single-core excitation. Additionally, the IC-XT distribution is also investigated in multi-core excitation conditions. The experimental validation of the theoretical model is performed in Section V with two different bending radius configurations showing good agreement with the herein presented nonlinear analysis. Finally, in Section VI the main conclusions of this work are highlighted.

Manuscript received January 25, 2016; revised March 15, 2016; accepted April 8, 2016. This work was supported by Spain the National Plan Project TEC2015-70858-C2-1-R XCORE and RTC-2014-2232-3 HIDRASENSE. The work of A. Macho was supported by BES-2013-062952 F.P.I. Grant. M. Morant was partly supported by UPV postdoc PAID-10-14 program.

A. Macho, M. Morant and R. Llorente are with Nanophotonics Technology Centre, Universitat Politècnica de València, 46022 Valencia, Spain, (e-mail: amachor@ntc.upv.es; mmorant@ntc.upv.es; rllorent@ntc.upv.es).

II. Unified Coupled-Mode Theory for MCF Media with Step-Index Coupled and Uncoupled Cores

The coupled-mode theory (CMT) was extended to nonlinear regime in [15] for uncoupled MCFs neglecting several mode-coupling coefficients (MCCs). However, this theoretical approximation should be further elaborated considering coupled cores, where the mode overlapping between the core modes is higher than in uncoupled MCFs [16], [17]. In this section, complete expressions of the coupled-mode equations are reported including additional MCCs for homogeneous and heterogeneous MCFs with coupled and uncoupled cores. The dominant MCCs are further investigated as a function of the core pitch value and the index mismatching between cores.

CMT unification for coupled and uncoupled MCFs operating in linear and nonlinear regime can be performed using a similar derivation as [18], [19] for the Homogeneous Nonlinear Directional Coupler (HNLDC). Nevertheless, the coupled-mode equations of the HNLDC are found to be inaccurate in heterogeneous MCFs with an intrinsic refractive index mismatching among cores and random perturbations of core modes due to fiber bending and twisting [7].

In order to propose a unified CMT in multi-core fiber media, a weakly guiding step-index two-core fiber (TCF) is considered in Fig. 1 for mathematical analysis. The TCF comprises two heterogeneous cores *n* and *m* assuming low nonlinear nature of silica media and monochromatic electric fields. In addition, neglecting fiber birefringence effects, a scalar approach is valid using the same polarization $\hat{\tau}$ in both cores considering that the mode coupling takes place between nonorthogonal polarizations. Hence, the complex amplitude of the global electric field (E_g) can be approximated to [18]–[20]:

$$\vec{E}_g(\vec{r}) \approx \vec{E}_n(\vec{r}) + \vec{E}_m(\vec{r}) = \begin{bmatrix} A_n(z) F_n(r,\varphi) \exp(-j\beta_n z) \\ +A_m(z) F_m(r,\varphi) \exp(-j\beta_m z) \end{bmatrix} \cdot \hat{\tau} \quad (1)$$

where $A_{n(m)}$ are the complex envelopes, $F_{n(m)}$ are the transversal functions of the LP_{01} mode in cores and cladding regions given by [21], $\beta_{n(m)}$ are the unperturbed phase constants of LP_{01} mode in cores *n* and *m*, and $\hat{\tau}$ is the unit vector modeling *x* or *y* polarization axis. From the Maxwell's equations, the nonlinear wave equation of the TCF can be expressed as [22]:

$$\Delta\vec{E}_g(\vec{r}) + k_0^2 \left[\varepsilon_{rg}(\vec{r}) + \alpha_{NL}(\vec{r}) \left| \vec{E}_g(\vec{r}) \right|^2 \right] \vec{E}_g(\vec{r}) = \vec{0} \quad (2)$$

where α_{NL} is related to the third-order nonlinear susceptibility of silica media as $\alpha_{NL} = 0.75 \cdot \chi^{(3)}$ and ε_{rg} is the relative electrical permittivity of the TCF, defined as:

$$\varepsilon_{rg}(\vec{r}) := \varepsilon_r(\vec{r}) + \Delta\varepsilon_{rn}(\vec{r}) + \Delta\varepsilon_{rm}(\vec{r}) \quad (3)$$

In addition, note that the transversal functions and exponential terms of Eq. (1) should satisfy the Helmholtz equation in each core. Thus, from the Helmholtz equation and using Eq. (3), the next relation is found in each core:

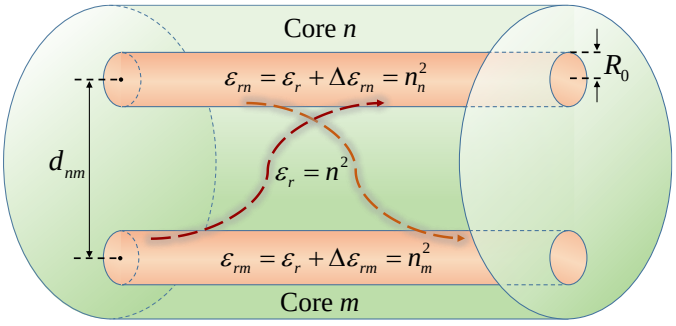

Fig. 1. Heterogeneous two-core fiber (TCF) media analyzed.

$$\Delta_T F_{n(m)} + k_0^2 \varepsilon_{rg} F_{n(m)} = \left[k_0^2 \Delta\varepsilon_{rm(n)} + \beta_{n(m)}^2 \right] F_{n(m)} \quad (4)$$

Thus, applying Eqs. (1) and (4) in Eq. (2), assuming the slowly varying envelope approximation with $A_n'' \approx A_m'' \approx 0$ in $\Delta z \approx \lambda$, multiplying the resultant equation by $F_n^*(r,\varphi)\cdot\exp(+j\beta_n z)$ and integrating in an infinite cross-sectional area with a similar mathematical derivation as in the classical nonlinear CMT [18], [19], we obtain:

$$\begin{aligned} j\left[\frac{dA_n}{dz} + \chi_{nm} \exp(-j\Delta\beta_{mn} z) \frac{dA_m}{dz} \right] = \\ = c_n A_n + k_{nm} \exp(-j\Delta\beta_{mn} z) A_m + q_{1n} |A_n|^2 A_n \\ + q_{2nm} \left[2A_n |A_m|^2 + A_n^* A_m^2 \exp(-j2\Delta\beta_{mn} z) \right] \\ + q_{3nm} \begin{bmatrix} 2|A_n|^2 A_m \exp(-j\Delta\beta_{mn} z) \\ +A_n^2 A_m^* \exp(+j\Delta\beta_{mn} z) \end{bmatrix} \\ + q_{4nm} |A_m|^2 A_m \exp(-j\Delta\beta_{mn} z) \end{aligned} \quad (5)$$

with $\Delta\beta_{mn} = \beta_m - \beta_n$. A similar equation modeling mode coupling from core *n* to core *m* can be obtained by repeating the procedure multiplying by $F_m^*(r,\varphi)\cdot\exp(+j\beta_m z)$. In addition, the MCCs of Eq. (5) for the LP_{01} mode are given by the next expressions (derivation detailed in Appendix):

$$\chi_{nm} = \frac{\beta_m}{\beta_n} \frac{\iint F_m F_n dS_\infty}{\iint F_n^2 dS_\infty} \approx \frac{2n_m}{n_n} \frac{J_0^2(u_n)}{\left[J_0^2(u_n) + J_1^2(u_n) \right]} \begin{bmatrix} \frac{J_1(u_n) K_0(w_m d_{nm}/R_0)}{u_n J_0(u_n) K_0(w_m)} \\ + \frac{J_1(u_m) K_0(w_n d_{nm}/R_0)}{u_m J_0(u_m) K_0(w_n)} \end{bmatrix} \quad (6a)$$

$$c_n = \frac{k_o^2}{2\beta_n} \frac{\iint \Delta\varepsilon_{rm} F_n^2 dS_\infty}{\iint F_n^2 dS_\infty} = \frac{k_o^2 NA_m^2}{2\beta_n} \frac{\iint F_n^2 dS_m}{\iint F_n^2 dS_\infty} \approx \frac{k_0 NA_m^2}{2n_n} \frac{K_0^2(w_n d_{nm}/R_0)}{K_0^2(w_n)} \frac{J_0^2(u_n)}{\left[J_0^2(u_n) + J_1^2(u_n) \right]} \quad (6b)$$

$$k_{nm} = \frac{k_o^2}{2\beta_n} \frac{\iint \Delta\varepsilon_{rn} F_m F_n dS_\infty}{\iint F_n^2 dS_\infty} = \frac{k_o^2 NA_n^2}{2\beta_n} \frac{\iint F_m F_n dS_n}{\iint F_n^2 dS_\infty} \approx \frac{k_0 NA_n^2}{n_n} \frac{J_0(u_n) J_1(u_n)}{u_n \left[J_0^2(u_n) + J_1^2(u_n) \right]} \frac{K_0(w_m d_{nm}/R_0)}{K_0(w_m)} \quad (6c)$$

$$q_{1n} = \frac{k_o^2}{2\beta_n} \frac{\iint \alpha_{NL} F_n^4 \mathrm{d}S_\infty}{\iint F_n^2 \mathrm{d}S_\infty} \approx \frac{k_0 \alpha_{NL} H_n^2}{8 n_n R_0^2} \frac{\left[1-\exp\left(-4R_0^2/H_n^2\right)\right]}{J_0^2(u_n)\left[J_0^2(u_n)+J_1^2(u_n)\right]} \quad (6d)$$

$$q_{2nm} = \frac{k_o^2}{2\beta_n} \frac{\iint \alpha_{NL} F_m^2 F_n^2 \mathrm{d}S_\infty}{\iint F_n^2 \mathrm{d}S_\infty} \approx \frac{k_0 \alpha_{NL}}{2 n_n} \left\{ \frac{K_0^2(w_m d_{nm}/R_0)}{K_0^2(w_m)} + \frac{J_0^2(u_n)}{J_0^2(u_m)} \cdot \frac{K_0^2(w_n d_{nm}/R_0)}{K_0^2(w_n)} \left[\frac{J_0^2(u_m)+J_1^2(u_m)}{J_0^2(u_n)+J_1^2(u_n)} \right] \right\} \quad (6e)$$

$$q_{3nm} = \frac{k_o^2}{2\beta_n} \frac{\iint \alpha_{NL} F_m F_n^3 \mathrm{d}S_\infty}{\iint F_n^2 \mathrm{d}S_\infty} \approx \frac{k_0 \alpha_{NL} H_n^2}{6 n_n R_0^2} \frac{K_0(w_m d_{nm}/R_0)}{J_0(u_n) K_0(w_m)} \left[\frac{1-\exp\left(-3R_0^2/H_n^2\right)}{J_0^2(u_n)+J_1^2(u_n)} \right] \quad (6f)$$

$$q_{4nm} = \frac{k_o^2}{2\beta_n} \frac{\iint \alpha_{NL} F_m^3 F_n \mathrm{d}S_\infty}{\iint F_n^2 \mathrm{d}S_\infty} \approx \frac{k_0 \alpha_{NL} H_m^2}{6 n_n R_0^2} \frac{J_0^2(u_n) K_0(w_n d_{nm}/R_0)}{J_0^3(u_m) K_0(w_n)} \left[\frac{1-\exp\left(-3R_0^2/H_m^2\right)}{J_0^2(u_n)+J_1^2(u_n)} \right] \quad (6g)$$

where R_0 is the core radius, $NA_{n(m)} = [n_{n(m)}^2 - n^2]^{1/2}$ is the numerical aperture of each core, $H_{n(m)}$ is the modal field radius of LP_{01} mode in cores n and m given by Eq. (2.2.15) of [22], and the modal parameters $u_{n(m)}$ and $w_{n(m)}$ can be calculated from [21]. The MCCs given by Eqs. (6) provide analytic expressions to estimate mode coupling between cores with different core pitch value and electrical permitivities assuming step-index and single-mode cores with identical core radius. Nevertheless, considering multi-mode regime or cores with different radius, gradual-index or trench assisted MCFs, Eqs. (6) should be revisited performing the same analytic derivation as detailed in Appendix.

The nonlinear MCCs can be classified in intramodal and intermodal nonlinear coupling effects [13], [14]. The intramodal effect is related with the self-coupling effect given by q_{1n} coefficient and intermodal effects are related with the cross-coupling effect given by q_{2nm}, q_{3nm} and q_{4nm} MCCs. As it was pointed out in [15], in uncoupled MCFs with large core pitch value, k_{nm} and q_{1n} are the dominant linear and nonlinear MCCs, respectively; and the additional MCCs can be neglected due to the low mode overlapping in these MCFs. However, this theoretical approximation should be further analyzed when changing the core pitch and the core refractive index in coupled and heterogeneous MCFs. Considering a TCF with fiber parameters: R_0 = 4 μm, n_m = 1.45, n = 1.44, $\alpha_{NL} = 8.13 \cdot 10^{-20}$ and λ =1550 nm; the linear MCCs χ_{nm} and c_n, and the nonlinear MCCs q_{2nm}, q_{3nm} and q_{4nm} are compared with the dominant linear and nonlinear MCCs k_{nm} and q_{1n}, respectively. The ratios χ_{nm}/k_{nm}, c_n/k_{nm}, q_{2nm}/q_{1n}, q_{3nm}/q_{1n} and q_{4nm}/q_{1n} were calculated using Eqs. (6).

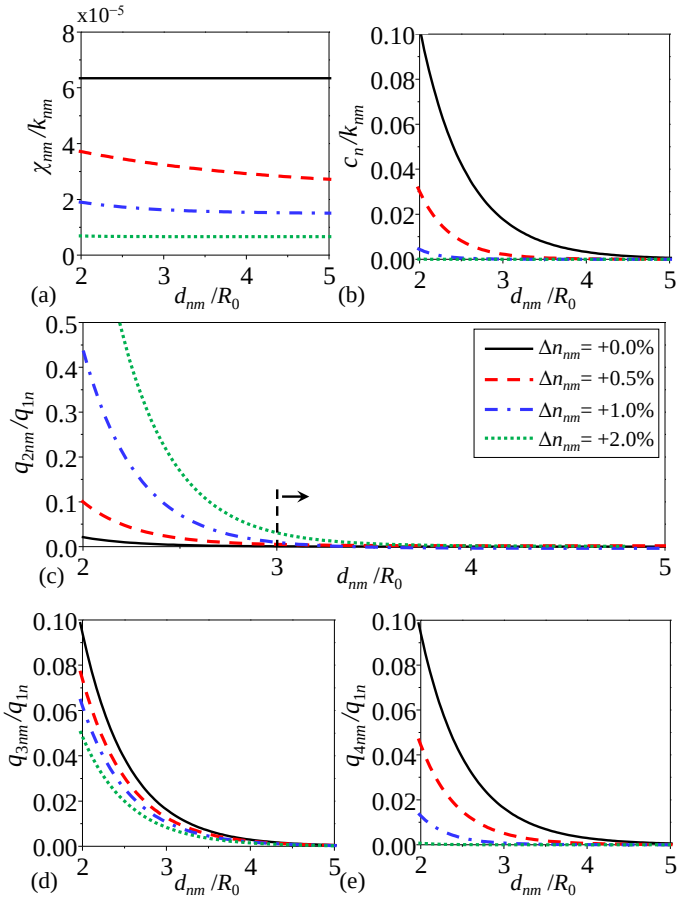

Fig. 2. Comparison of the linear mode-coupling coefficients (MCCs) χ_{nm} and c_n and the nonlinear MCCs q_{2nm}, q_{3nm} and q_{4nm} with the dominant linear and nonlinear MCCs k_{nm} and q_{1n} for different core pitch ratio d_{nm}/R_0 and index mismatching values $\Delta n_{nm} = (n_n - n_m)/n_m$ between cores n and m. MCC ratios: (a) χ_{nm}/k_{nm}, (b) c_n/k_{nm}, (c) q_{2nm}/q_{1n}, (d) q_{3nm}/q_{1n}, and (e) q_{4nm}/q_{1n}.

Fig. 2 shows the behaviour of these MCC ratios with different index mismatching values $\Delta n_{nm} = (n_n - n_m)/n_m$ varying n_n and with different ratio between the core pitch and the core radius d_{nm}/R_0. The analysis considering $\Delta n_{mn} = (n_m - n_n)/n_n$ varying n_m was not included in Fig. 2 because the conclusions in the behaviour of the MCC ratios were found identical.

It can be noticed from Fig. 2 that χ_{nm}, c_n, q_{2nm}, q_{3nm} and q_{4nm} MCCs can be omitted for any core pitch value in homogeneous coupled and uncoupled MCF media. Additionally, in heterogeneous MCFs with $\Delta n_{nm} > 0\%$ it can be observed that the higher the index mismatching term Δn_{nm}, the lower the MCC ratios depicted in Figs. 2(a), (b), (d) and (e). Therefore, χ_{nm}, c_n, q_{3nm} and q_{4nm} MCCs can also be neglected in MCF media with heterogeneous coupled and uncoupled cores. However, as depicted in Fig. 2(c), the ratio q_{2nm}/q_{1n} increases as the index mismatching term Δn_{nm} increases. Hence, in coupled heterogeneous MCFs with $2R_0 < d_{nm} < 3R_0$ and large index mismatching term ($\Delta n_{nm} > 1$ %), q_{2nm} coefficient should be maintained in Eq. (5) considering that $q_{2nm} >> 0.1 \cdot q_{1n}$, as shown in Fig. 2(c). Consequently, in coupled and heterogeneous MCFs with low core pitch value the nonlinear MCC q_{2nm} cannot be neglected.

Moreover, an additional consideration should be pointed out for the linear k_{nm} mode-coupling coefficient. In [23] and [24]

Snyder and Okamoto reported an analogous closed-form expression for the linear k_{nm} coefficient considering identical modal parameters $u_n = u_m$ and $w_n = w_m$ in each core. This approximation can be applied to homogeneous MCFs. Nevertheless, the closed-form expression depicted in Eq. (6c) for k_{nm} coefficient improves the accuracy of these references in heterogeneous cores with $u_n \neq u_m$ and $w_n \neq w_m$.

In order to complete the theoretical CMT unification in MCF, macrobends and structural fluctuations of the media inducing random perturbations in the phase constants of core modes should be included in Eq. (5). In coherence with [12] the exponential terms can be rewritten as:

$$\exp\left[-j\Delta\phi_{mn}(z)\right] = \exp\left[-j\left(\int_0^z \Delta\beta_{eq,mn}(\tau)\,\mathrm{d}\tau\right)\right] \quad (7)$$

where $\Delta\beta_{eq,mn}$ includes phase-mismatching effect due to bends and structural fluctuations inducing perturbations in the phase constants β_n and β_m. Considering constant bending radius (R_b) and random twist rate along the MCF length, the phase-mismatching term $\Delta\phi_{mn}(z)$ can be expressed as [25]:

$$\Delta\phi_{mn}(z) = (\beta_m - \beta_n)\,z - \frac{\beta_n d_{nm}}{R_b}\int_0^z \cos\left(\theta_{nm}(\delta)\right)\mathrm{d}\delta \quad (8)$$

where d_{nm} is the core pitch between cores n and m, and θ_{nm} is the random twist angle described by a real spatial random process. Finally, the unified coupled-mode equation for heterogeneous and homogenous, coupled and uncoupled N-core MCF with $d_{nm} > 2R_0$ operating in linear and nonlinear regime is reduced to:

$$j\frac{\mathrm{d}A_n}{\mathrm{d}z} = q_{1n}|A_n|^2 A_n + \sum_{m\neq n}^{N}\left\{\begin{array}{l} k_{nm}A_m\exp(-j\Delta\phi_{mn}) + \\ +q_{2nm}\left[2A_n|A_m|^2 + A_n^* A_m^2\exp(-j2\Delta\phi_{mn})\right]\end{array}\right\} \quad (9)$$

The behaviour of the linear and nonlinear crosstalk was compared performing a numerical simulation of the crosstalk from core m to core n defined as $10\cdot\log(|A_n|^2/|A_m|^2)$ using Eqs. (8) and (9). Two different core pitch values were considered in the simulations with $d_{nm} = 10R_0$ and $d_{nm} = 2.5R_0$ in order to analyze both uncoupled and coupled cores, respectively. The numerical results of each case are depicted in Figs. 3(a) and (b). It was assumed a heterogeneous TCF with constant bending radius R_b = 50 cm, R_0 = 4 μm, n = 1.44, n_m = 1.45, n_n = 1.46, λ = 1550 nm, $\alpha_{NL} = 8.13\cdot10^{-20}$ m^2/W and Gaussian random fiber twisting in $\theta_{nm}(z)$ in Eq. (8). The linear and nonlinear inter-core crosstalk were simulated considering as initial conditions an optical power launch level of $P_L = |A_m(z=0)|^2_{(\mathrm{dBm})}$ = 0 dBm and 25 dBm, respectively. The green line describes the longitudinal evolution of the linear crosstalk, the black line depicts the longitudinal evolution of the nonlinear crosstalk considering only the q_{1n} nonlinear MCC in Eq. (9) and the red line describes the same result considering both q_{1n} and q_{2nm} nonlinear MCCs in Eq. (9).

As depicted in Figs. 3(a) and (b), the linear and nonlinear crosstalk present a random evolution along the MCF length. However, in nonlinear regime (red and black lines) the crosstalk is reduced due to the additional phase mismatching induced in core m by the stimulation of the Kerr effect. Furthermore, it should be noticed that in Fig. 3(a) we cannot observe any difference in the solution of Eq. (9) when q_{2nm} is neglected or maintained. In contrast, in coupled heterogeneous MCFs with a reduced core pitch ($d_{nm} < 3R_0$) the nonlinear MCC q_{2nm} should be retained as indicated in Fig. 2(c) and confirmed in Fig. 3(b). The numerical solution shows that in a heterogeneous coupled MCF, when the mode overlapping between cores is high, the cross-coupling effect increases the nonlinear crosstalk and, therefore, it should be included in the nonlinear coupled-mode equation Eq. (9).

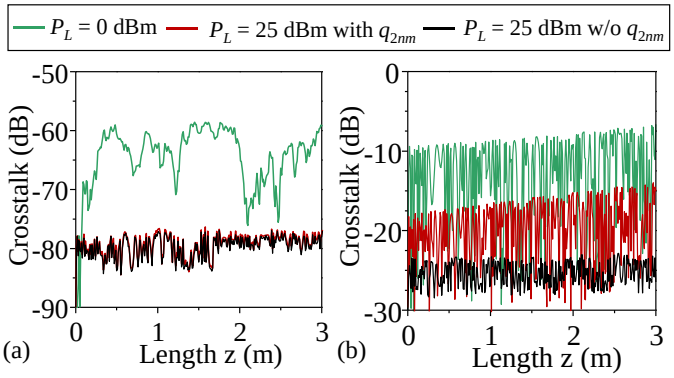

Fig. 3. Simulation results of the crosstalk longitudinal evolution using Eq. (9) in a heterogeneous two-core fiber for different power launch levels (P_L) and different core pitch values (d_{nm}) considering: (a) d_{nm}=10·R_0 and (b) d_{nm}=2.5·R_0. Green line: linear crosstalk with P_L=0dBm, Red line: nonlinear crosstalk with P_L=25dBm including q_{2nm} in Eq. (9), Black line: nonlinear crosstalk with P_L=25dBm neglecting q_{2nm} in Eq. (9).

The unified coupled-mode theory permits to estimate the average value of the linear and nonlinear crosstalk in MCF media performing a Monte Carlo simulation using Eq. (9). However, the exponential terms including phase information increase the computational complexity of the numerical simulations. In order to investigate in the next sections a closed form expression for estimating the average value of the nonlinear crosstalk without using numerical simulations, the coupled-power theory [9] should be previously revisited in nonlinear regime.

III. Nonlinear Coupled-Power Theory

Coupled-power theory (CPT) proposed by Dietrich Marcuse for multi-mode fibers [26] has been revisited by Koshiba for MCFs when operating in linear regime [9]. In order to propose in Section IV the closed-form expressions to estimate the mean and variance of the nonlinear crosstalk, the CPT is extended to nonlinear regime in this section. From now on, we consider in the theoretical analysis the prevailing fiber design criteria $d_{nm} > 4R_0$ in high-capacity SDM transmissions using MCF media [16], [17], [27].

In linear regime, the crosstalk in a N-core MCF can be written as a function of the power exchange among cores as [7], [9]:

$$\frac{\mathrm{d}P_n(z)}{\mathrm{d}z} = -\alpha_{att}P_n(z) + \sum_{n\neq m}^{N} h_{nm}\left[P_m(z) - P_n(z)\right] \quad (10)$$

where α_{att} is the power attenuation coefficient of the MCF and h_{nm} is the power coupling coefficient describing linear crosstalk from core m to core n. The power coupling coefficient h_{nm} takes into account the random perturbations of the MCF, as detailed in [7] and [9]. However, in nonlinear regime the Kerr effect reducing the mode coupling among cores should be included in Eq. (10). As we have previously demonstrated in Section II, the dominant nonlinear effect in coupled and uncoupled MCFs with the core pitch higher than three times the core radius is the self-coupling effect given by q_{1n} coefficient. Hence, in order to estimate the nonlinear crosstalk using a first-order solution of the nonlinear CMT, additional nonlinear effects given by q_{2nm}, q_{3nm} and q_{4nm} coefficients can be neglected considering MCF media with $d_{nm} > 3R_0$. Consequently, the corresponding self-coupling power coefficient h_n can be investigated reducing Eq. (9) to:

$$\frac{\mathrm{d}}{\mathrm{d}z}\mathbf{A}(z) = -j\cdot\mathbf{M}(z)\cdot\mathbf{A}(z) \quad (11a)$$

with the **M** matrix defined as:

$$\mathbf{M}(z) := \mathbf{q}\cdot\mathbf{P_e}(z) + \\ + \exp\left(j\int_0^z \boldsymbol{\beta}_{\mathbf{eq}}(\tau)\,\mathrm{d}\tau\right)\cdot\mathbf{k}\cdot\exp\left(-j\int_0^z \boldsymbol{\beta}_{\mathbf{eq}}(\tau)\,\mathrm{d}\tau\right) \quad (11b)$$

where $\mathbf{q} = diag(q_{11},\ldots,q_{1N})$ is the *NxN* diagonal matrix of self-modulation coupling coefficients; $\mathbf{A}(z) = [A_1(z),\ldots,A_N(z)]^{\mathrm{T}}$ is the vector of the complex envelopes; $\boldsymbol{\beta}_{\mathbf{eq}}$ is the *NxN* diagonal matrix with the equivalent phase constants; $\mathbf{P_e} = diag(P_1,\ldots,P_N)$ is the *NxN* diagonal matrix including the complex envelope power; and **k** is the *NxN* matrix with the mode-coupling coefficients k_{nm}. Based on the perturbation theory [26] and assuming low crosstalk conditions with the coupled power of the complex envelope approximately constant when operating in nonlinear regime, Eq. (11a) admits a first-order solution of the form:

$$\mathbf{A}(z) \approx \left(\mathbf{I} - j\int_0^z \mathbf{M}(z')\,\mathrm{d}z'\right)\cdot\mathbf{A}(0) \quad (12)$$

where **I** is the identity matrix. Thus, analyzing a MCF section with N cores between z_1 and z_2 with $|z_2-z_1|$ larger than the correlation length of the crosstalk, the evolution of the complex envelopes along the MCF can be written as $\mathbf{A}(z_2) = \mathbf{T}\cdot\mathbf{A}(z_1)$, where **T** is the *NxN* transfer matrix of the complex envelopes in the MCF section. This matrix is given by:

$$\mathbf{T} \approx \mathbf{I} - j\int_{z_1}^{z_2} \mathbf{M}(z')\,\mathrm{d}z' \quad (13)$$

Therefore, the evolution of the complex envelope from core m to core n is described by the T_{nm} coefficient:

$$T_{nm} \approx \begin{cases} 1 - jq_{1n}\int_{z_1}^{z_2} P_n(z')\,\mathrm{d}z'; & \text{if } n = m \\ -jk_{nm}\int_{z_1}^{z_2}\exp\left[-j\int_{z_1}^{z'}\left(\beta_{eq,m}-\beta_{eq,n}\right)\mathrm{d}\tau\right]\mathrm{d}z'; & \text{if } n \neq m \end{cases} \quad (14)$$

It can be noticed in Eq. (14) that T_{nm} coefficient describes the linear crosstalk when $n \neq m$. As it has been demonstrated in [7], [9], the power coupling coefficient h_{nm} describing linear mode coupling from core m to core n in Eq. (10) can be derived from T_{nm} coefficient as:

$$h_{nm} = \frac{\left\langle |T_{nm}|^2 \right\rangle}{z_2 - z_1} \approx k_{nm}^2 S_f\left(\upsilon = \frac{\Delta\beta_{mn}}{2\pi}\right) \quad (15)$$

where $\langle\ \rangle$ is the ensemble average operator; S_f is the power spectral density (PSD) function of the $f(z)$ random process modeling macrobends and structural fluctuations of the MCF media [7], [9]; and υ is the spatial frequency. On the other hand, with $n = m$ in Eq. (14), T_{nn} coefficient involves the linear propagation of the LP_{01} mode and the self-coupling effect:

$$T_{nn} = \underset{\text{Linear propagation}}{1} \underbrace{-jq_{1n}\int_{z_1}^{z_2} P_n(z')\,\mathrm{d}z'}_{\text{Self-Coupling Effect}} \quad (16)$$

Therefore, the self-coupling power coefficient h_n can be written in the MCF section as:

$$h_n = \frac{\left\langle |T_{nn}|^2 \right\rangle - 1}{z_2 - z_1} = \frac{\left\langle T_{nn}\cdot T_{nn}^* \right\rangle - 1}{z_2 - z_1} \\ = \frac{1}{z_2 - z_1} q_{1n}^2 \int_{z=z_1}^{z_2}\int_{z'=z_1}^{z_2} \left\langle P_n(z) P_n^*(z')\right\rangle \mathrm{d}z'\mathrm{d}z \\ = \frac{1}{z_2 - z_1} q_{1n}^2 \int_{z=z_1}^{z_2}\int_{z'=z_1}^{z_2} R_{pn}(z'-z)\,\mathrm{d}z'\mathrm{d}z \quad (17)$$

where $R_{pn}(z'-z)$ is the autocorrelation function (ACF) of the coupled power P_n. Performing the dummy variable transformation $\tau = z'-z$ and considering the correlation length of $R_{pn}(\tau)$ shorter than the MCF section length $|z_2-z_1|$, the integral in τ can be approximated to the Spatial Fourier Transform. From the Wiener-Khinchin theorem, the PSD function of $R_{pn}(\tau)$ can be defined as [28]:

$$S_{pn}(\upsilon) = \int_{-\infty}^{+\infty} R_{pn}(\tau)\exp(+j2\pi\upsilon\tau)\,\mathrm{d}\tau \quad (18)$$

and finally, the self-coupling power coefficient can be written as:

$$h_n = \frac{1}{z_2 - z_1} q_{1n}^2 \int_{z=z_1}^{z_2}\int_{\tau=z_1-z}^{z_2-z} R_{pn}(\tau)\,\mathrm{d}\tau\mathrm{d}z \\ \approx q_{1n}^2 \int_{\tau=-\infty}^{+\infty} R_{pn}(\tau)\,\mathrm{d}\tau = q_{1n}^2 S_{pn}(\upsilon = 0) \quad (19)$$

Considering that the self-coupling effect reduces the power coupling between cores, as it is experimentally verified in Section V, the power coupling coefficient h_{nm} is modified as:

$$h_{nm,eq} = h_{nm} - h_n \approx k_{nm}^2 S_f\left(\Delta\beta_{mn}/2\pi\right) - q_{1n}^2 S_{pn}(0) \quad (20a)$$

Therefore, the coupled-power equation Eq. (10) is rewritten in nonlinear regime considering a *N*-core MCF as:

$$\frac{\mathrm{d}P_n(z)}{\mathrm{d}z} = -\alpha_{att} P_n(z) + \sum_{\substack{n=1 \\ n\neq m}}^{N} h_{nm,eq}\left[P_m(z) - P_n(z)\right] \quad (20b)$$

In order to complete the statistical model of the crosstalk in MCF, Eqs. (20) can be used to estimate theoretically the mean and variance of the crosstalk in nonlinear regime, as detailed in Section IV and validated experimentally in Section V.

IV. Statistical Model and Theoretical Estimation of Nonlinear Crosstalk

Aimed to unify the IC-XT statistical models reported in [12] and [15], the closed-form expressions for estimating the cumulative distribution function (cdf), and the mean and variance of the linear and nonlinear crosstalk are derived in this section. From [15], the probability density function (pdf) of the nonlinear crosstalk in MCF media can be expressed as:

$$f_{X_{nm}^{NL}}(x_{NL}) = \frac{\left(12L^4 q_{1n}^4 P_L^4 x_{NL}^5 + 16L^2 q_{1n}^2 P_L^2 x_{NL}^3 + 4x_{NL}\right)}{N_{NL}^2 \left|K_{nm}\right|^4} \cdot \cdot \exp\left(-\frac{L^2 q_{1n}^2 P_L^2 x_{NL}^3 + x_{NL}}{N_{NL}\left|K_{nm}\right|^2/2}\right) \cdot u(x_{NL}) \quad (21)$$

where N_{NL} is the *N-th* phase-matching points between cores *n* and *m* in nonlinear regime, L is the MCF length, P_L is the optical power launch level, K_{nm} is the linear coupling coefficient for the discrete changes [12], X_{NL} is the nonlinear crosstalk random variable (r.v.) and $u(x)$ is the unit step function. Moreover, the cdf, mean and variance of the nonlinear crosstalk can be calculated considering [12], [15]: (i) the cdf of the linear crosstalk; (ii) the cubic relation between the linear crosstalk (x_L) and the nonlinear crosstalk (x_{NL}) given by $x_L = h(x_{NL}) = L^2 q_{1n}{}^2 P_L{}^2 x_{NL}{}^3 + x_{NL}$, where h is a bijective and positive-real function in the domain $x_{NL} \geq 0$; and (iii) the relation of the nonlinear crosstalk r.v. with the standard chi-squared distribution (χ_4^2) with 4 degrees of freedom (d.f.) given by the expression $X_{nm}{}^{NL} \approx (N_{NL} \cdot K_{nm}/4) \cdot \chi_4^2$. Thus:

$$\begin{aligned} F_{X_{nm}^{NL}}(x_{NL}) &= P\left(X_{nm}^{NL} \leq x_{NL}\right) = P\left(h^{-1}\left(X_{nm}^{L}\right) \leq x_{NL}\right) \\ &= P\left(X_{nm}^{L} \leq h(x_{NL})\right) = F_{X_{nm}^{L}}\left(h(x_{NL})\right) \\ &= \left[1 - \left(1 + \frac{2L^2 q_{1n}^2 P_L^2 x_{NL}^3 + 2x_{NL}}{N_{NL}\left|K_{nm}\right|^2}\right) \cdot \right. \\ &\quad \left. \cdot \exp\left(-\frac{2L^2 q_{1n}^2 P_L^2 x_{NL}^3 + 2x_{NL}}{N_{NL}\left|K_{nm}\right|^2}\right)\right] \cdot u(x_{NL}) \end{aligned} \quad (22)$$

$$\mu_{NL,nm} \approx N_{NL}\left|K_{nm}\right|^2 \quad (23)$$

$$\sigma_{NL.nm}^2 \approx N_{NL}^2 \left|K_{nm}\right|^4 / 2 \quad (24)$$

It can be noticed that the mean and variance of the nonlinear crosstalk cannot be estimated using Eqs. (23) and (24) because the number of phase-matching points N_{NL} is unknown. Nevertheless, in order to estimate these statistical parameters, their closed-form expressions can be additionally derived from the nonlinear coupled-power equation Eq. (20b). Assuming a TCF with $\alpha_{att} \approx 0$ where only the core *m* is excited and using Eq. (20b), we can write:

$$P_n(L) \approx P_n(0) + \int_0^L \left(h_{nm} - h_n\right)\left[P_m(z) - P_n(z)\right]\mathrm{d}z \quad (25)$$

Therefore, using Eq. (20a) and considering low crosstalk and short fiber lengths where the Kerr effect is stimulated, the optical attenuation can be neglected and we can approximate $P_m - P_n \approx P_m \approx \overline{P_m} \approx P_L$ in any z point, where the overbar represents the average value. Hence, the nonlinear mean defined as $\mu_{NL,nm} := E[P_n(L)/P_m(L)]$ can be approximated to:

$$\begin{aligned} \mu_{NL,nm} &\approx E\left[\frac{1}{P_m(L)}\left(\int_0^L h_{nm}\left[P_m(z) - P_n(z)\right]\mathrm{d}z \right.\right. \\ &\quad \left.\left. - \int_0^L q_{1n}^2 S_{pn}(0)\left[P_m(z) - P_n(z)\right]\mathrm{d}z\right)\right] \\ &\approx L\bar{h}_{nm} - Lq_{1n}^2 P_L E\left[\frac{S_{pn}(0)}{\overline{P_m}}\right] \\ &= L\bar{h}_{nm} - Lq_{1n}^2 P_L E\left[\frac{1}{\overline{P_m}}\int_{-\infty}^{+\infty}\left\langle P_n(z) P_n(z+\tau)\right\rangle \mathrm{d}\tau\right] \end{aligned} \quad (26)$$

where $E[\cdot]$ is the expectation operator. Note that $P_n(z)$ is an ergodic process, where the spatial averages of sample functions of the process are equal to the corresponding statistical averages. Consequently, Eq. (26) can be written as:

$$\begin{aligned} \mu_{NL,nm} &\approx L\bar{h}_{nm} - Lq_{1n}^2 P_L E\left[\frac{1}{\overline{P_m}}\int_{-\infty}^{+\infty} E\left[P_n(z) P_n(z+\tau)\right]\mathrm{d}\tau\right] \\ &= L\bar{h}_{nm} - Lq_{1n}^2 P_L E\left[\frac{P_n(z)}{\overline{P_m}}\int_{-\infty}^{+\infty} P_n(z+\tau)\,\mathrm{d}\tau\right] \end{aligned} \quad (27)$$

The last identity in the right-hand side (RHS) of Eq. (27) is performed considering the linear property of the expectation operator. Furthermore, as it is experimentally demonstrated in Section V, the variance of the crosstalk decreases in nonlinear regime. The random fluctuations of the coupled power $P_n(z)$ are minimized and, therefore, we can approximated $P_n(z)/\overline{P_m} \approx \mu_{NL,nm}$. As a result:

$$\begin{aligned} \mu_{NL,nm} &\approx L\bar{h}_{nm} - Lq_{1n}^2 P_L \mu_{NL,nm} E\left[\int_{-\infty}^{+\infty} P_n(z')\,\mathrm{d}z'\right] \\ &= L\bar{h}_{nm} - Lq_{1n}^2 P_L \mu_{NL,nm} \bar{P}_n(0) \end{aligned} \quad (28)$$

where the dummy variable change $z' = z+\tau$ is performed in the RHS of Eq. (28) and $\bar{\mathcal{P}}_n(0)$ is the average value of the Fourier Transform of $P_n(z')$ in $\upsilon = 0$. In general, the product $q_{1n}^2\bar{\mathcal{P}}_n(0)$ depends on additional parameters as the power launch value. Nevertheless, as it is verified experimentally in Section V, $q_{1n}^2\bar{\mathcal{P}}_n(0)$ can be approximated by a positive-real constant b assuming a slowly varying evolution with the power launch level. In addition, taking into account that $L\bar{h}_{nm}$ is the mean of the linear crosstalk $\mu_{L,nm}$ [7], Eq. (28) can be reduced to:

$$\mu_{NL,nm} \approx \mu_{L,nm} - bLP_L\mu_{NL,nm} \tag{29}$$

The mean and variance of the linear crosstalk can be written as a function of the number of phase-matching points N_L as $\mu_{L,nm} = N_L{\cdot}|K_{nm}|^2$ and $\sigma^2_{L,nm} = N_L{}^2{\cdot}|K_{nm}|^4/2$ [10]. Thus, it can be noted that the variance of the linear crosstalk is half of the crosstalk mean squared. Consequently, using Eqs. (23), (24) and (29), the closed-form expressions for estimating the crosstalk mean ($\mu_{NL,nm}$), variance ($\sigma^2_{NL,nm}$) and the number of phase-matching points (N_{NL}) in nonlinear regime are found as:

$$\mu_{NL,nm} \approx \frac{\mu_{L,nm}}{1+bLP_L} \tag{30}$$

$$\sigma^2_{NL.nm} \approx \frac{\mu^2_{NL,nm}}{2} \approx \frac{\mu^2_{L,nm}}{2\left(1+bLP_L\right)^2} = \frac{\sigma^2_{L.nm}}{\left(1+bLP_L\right)^2} \tag{31}$$

$$N_{NL} \approx \frac{\mu_{NL,nm}}{\left|K_{nm}\right|^2} \approx \frac{\mu_{L,nm}}{\left|K_{nm}\right|^2\left(1+bLP_L\right)} = \frac{N_L}{1+bLP_L} \tag{32}$$

with $P_L \geq P_c$, where $P_c \approx 2$ dBm is the critical optical power in silica MCF media [15]. The statistical parameters of linear crosstalk $\mu_{L,nm}$, $\sigma^2_{L,nm}$ and N_L can be estimated as a function of the fiber parameters from [10], [11]. The expressions given by Eqs. (21)-(32) unify the theoretical analysis of linear and nonlinear crosstalk in MCF media assuming single-core excitation condition.

However, considering multi-core excitation, the previous analysis can also be used to analyze the crosstalk distribution. If we assume that N cores are illuminated in a MCF, the mode coupling from the non-adjacent cores to an unexcited core i can be neglected, as depicted in Fig. 4. Consequently, assuming that the crosstalk is only increased by M adjacent cores (with $M < N$), the crosstalk in core i is modeled by the Y random variable, defined as:

$$Y := \frac{P_i(z=L)}{\sum_{j=1}^{M} p_j(z=L)} = \frac{\sum_{j=1}^{M} p_{ij}(z=L)}{\sum_{j=1}^{M} p_j(z=L)} \approx \frac{M\cdot p_{ij}(z=L)}{\sum_{j=1}^{M} p_j(z=L)} \tag{33}$$

where $P_i(z = L)$ is the total output power in core i, $p_j(z = L)$ is the output power in the excited core j and $p_{ij}(z = L)$ is the coupled power from core j to core i at the fiber output. Assuming adjacent cores with the same core pitch to core i, we can approximate $P_i(z = L) \approx M{\cdot}p_{ij}(z = L)$. In addition, IC-XT from core j to core i is given by $X_{ij} = p_{ij}(z = L)/p_j(z = L)$. Thus, Y and X_{ij} random variables can be related as:

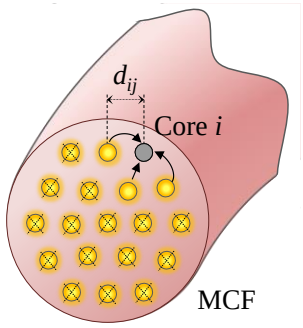

Fig. 4. Multi-core excitation in MCF media. The crosstalk in core i is increased by adjacent cores.

$$\frac{1}{Y} \approx \frac{1}{M\cdot p_{ij}(z=L)}\sum_{j=1}^{M} p_j(z=L) = \frac{1}{M}\sum_{j=1}^{M}\frac{p_j(z=L)}{p_{ij}(z=L)} = \frac{1}{M}\sum_{j=1}^{M}\frac{1}{X_{ij}} \tag{34}$$

From Eq. (34) and assuming independent X_{ij} r.v.s. considering low mode coupling among cores, the crosstalk distribution of core i can be found performing the following derivation. The pdf of the $Z_{ij} = 1/X_{ij}$ with $X_{ij} \geq 0$ can be written as:

$$f_{Z_{ij}}(z_{ij}) = f_{X_{ij}}\left(\frac{1}{z_{ij}}\right)\left|\frac{d}{dz_{ij}}\left(\frac{1}{z_{ij}}\right)\right| = \frac{1}{z_{ij}^2} f_{X_{ij}}\left(\frac{1}{z_{ij}}\right) \tag{35}$$

In addition, defining a new random variable $W = \sum Z_{ij}$, the pdf $f_W(w)$ is given by [28]:

$$f_W(w) = f_{Z_{i1}}(w) * \ldots * f_{Z_{iM}}(w) = \left[\frac{1}{w^2} f_{X_{i1}}\left(\frac{1}{w}\right)\right] * \ldots * \left[\frac{1}{w^2} f_{X_{iM}}\left(\frac{1}{w}\right)\right] \tag{36}$$

where $*$ is the convolution operation. From Eq. (36) we can found the pdf of the random variable $U = 1/W$ as:

$$f_U(u) = f_W\left(\frac{1}{u}\right)\left|\frac{d}{du}\left(\frac{1}{u}\right)\right| = \frac{1}{u^2}\left\{\left[u^2 f_{X_{i1}}(u)\right] * \ldots * \left[u^2 f_{X_{iM}}(u)\right]\right\} \tag{37}$$

where $f_{Xij}(u)$ is given by Eq. (21). Finally, the pdf of the random variable $Y = M{\cdot}U$ is derived from Eq. (37):

$$f_Y(y) = f_U\left(\frac{y}{M}\right)\left|\frac{d}{dy}\left(\frac{y}{M}\right)\right| = \frac{1}{M^{2M-1}y^2}\left\{\left[y^2 f_{X_{i1}}\left(\frac{y}{M}\right)\right] * \ldots * \left[y^2 f_{X_{iM}}\left(\frac{y}{M}\right)\right]\right\} \tag{38}$$

As detailed in Eq. (38), the crosstalk distribution when operating with multi-core excitation condition can be estimated from the IC-XT model depicted in Eqs. (21)-(32). As it is experimentally verified in Section V, the pdf of the crosstalk given by Eq. (38) can also be identified as a chi-squared distribution. However, the degrees of freedom of the crosstalk distribution can be increased more than 4 degrees

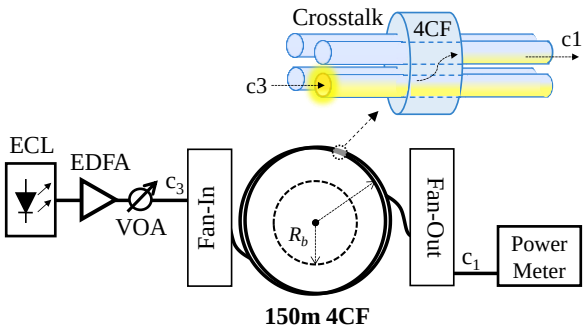

Fig. 5. Experimental set-up employed for linear and nonlinear crosstalk evaluation in single-core excitation condition.

due to the $M-1$ convolution operations. The mathematical interpretation is found in the increment of the crosstalk variance due to the convolution operation. Moreover, the physical interpretation is related to the increment of the number of phase-matching points in core i due to the excitation of the adjacent cores.

V. Experimental Validation

In order to validate the theoretical analysis reported in previous sections, experimental measurements are performed on homogeneous MCF with 4 cores analyzing the crosstalk statistics in linear and nonlinear regimes when considering both single-core and multi-core excitation.

The statistical analysis of the crosstalk in single-core excitation condition is experimentally evaluated on 150 m of 4CF with a constant twist rate of 4 turns/m and two different bending radius (R_b) configurations of 67 and 100 cm, as shown in Fig. 5. A tunable external cavity laser (ECL) at 1550 nm with a linewidth of 50 kHz was used with optical amplification performed with an erbium doped fiber amplifier (EDFA). The EDFA gain is maximized in order to minimize the noise factor to reduce the crosstalk averaging due to amplified spontaneous emission (ASE) noise [15]. A variable optical attenuator (VOA) was employed to modify the optical power level launched into the fiber ranging from −3 dBm to 18 dBm taking into account the insertion loss of the 3D fan-in device measured in 2.2 dB. As depicted in Fig. 5, the optical power was injected into core 3 and measured in core 1 with an optical power meter (Newport 1931-C). In addition, it should be noticed that the stimulated Brillouin scattering (SBS) does not reflect any portion of the power injected in the 150 m of 4CF when operating with a power launch level lower than 20 dBm considering that the SBS threshold power is estimated in 23.5 dBm in our 150 m of 4CF. The cdf, pdf, mean and variance of the linear and nonlinear crosstalk were estimated from more than 6000 samples of crosstalk for each power launch value using the wavelength sweeping method [29] from 1550 to 1580 nm with 5 pm step.

Fig. 6 shows the experimental evaluation considering single-core excitation of the IC-XT mean, variance and the number of phase-matching points as a function of the optical power launched into core 3. In linear regime, the crosstalk statistical parameters are constant with the optical power

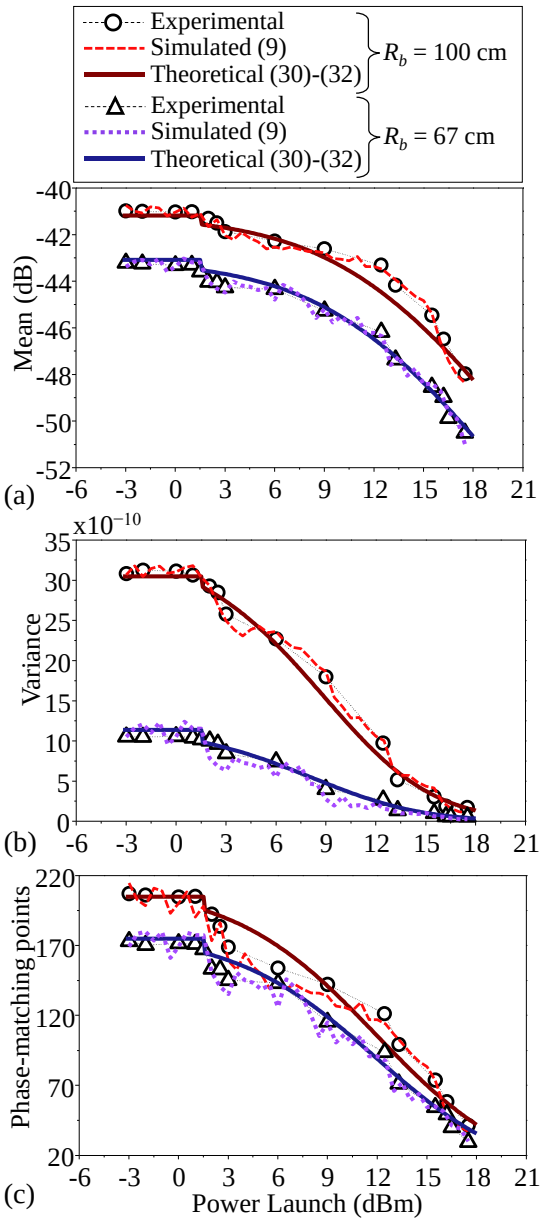

Fig. 6. Statistical analysis of inter-core crosstalk mean, variance and number of phase-matching points as function of the power launch level for two different bending radius (R_b). Circles: measured data for R_b = 100 cm. Triangles: measured data for R_b = 67 cm.

launch level. However, in nonlinear regime Kerr effect detunes the phase constant of core modes as the power launch level is increased in a single core and, therefore, the homogeneous 4CF becomes heterogeneous. As a result, the mean, variance and the number of phase-matching points of the crosstalk is reduced in nonlinear regime, as confirmed in Figs. 6(a), (b) and (c), respectively.

Due to the reduction of the number of phase-matching points (N_{NL}) when the optical power launch level increases, the crosstalk mean also decreases in presence of fiber Kerr nonlinearities. This is confirmed in Fig. 6(a) with a reduction of the crosstalk mean between both power regimes from −43 dB to −50 dB with R_b = 67 cm, and from −41 dB to −49 dB with R_b = 100 cm. The variance of the crosstalk distribution is also reduced in nonlinear regime, as it can be

observed in Fig. 6(b). The variance decreases for power launch levels higher than 2 dBm and it stabilizes at around 15 dBm for the two bending radius configurations evaluated. Consequently, the crosstalk cannot be considered as a strict-sense stationary random process in nonlinear regime if the power launch conditions are temporally modified.

The statistical parameters of the crosstalk can be estimated in both linear and nonlinear power regimes using two different strategies: (i) performing a Monte Carlo simulation using the CMT reported in Section II and, (ii) using the closed-form expressions derived in Section IV. The two proposed strategies for estimating the crosstalk statistical parameters in both power regimes were validated with the experimental results.

A Monte Carlo simulation was performed using Eq. (9) over 500 iterations for each power launch level considering longitudinal Gaussian random fluctuations in the average value of the core radius (R_0), fiber bending radius (R_b) and twist rate around ~0.1 μm, ~1 m and ~0.2 turns/m, respectively. The random fluctuations of these fiber parameters induce stochastic variations in the equivalent refractive index of each core around ~10^{-5}. The power launch level was modified in the simulation from −3 dBm to 18 dBm with 0.5 dB step. The comparison between the measured and the simulated results is depicted in Fig. 6. It can be noticed that the Monte Carlo simulation fits correctly with the experimental measurements for each bending radius configuration validating the coupled-mode equation Eq. (9) reported in Section II. In addition, it should be remarked that the fluctuation of the Monte Carlo simulation results can be reduced increasing the number of iterations.

Moreover, the crosstalk statistical parameters can also be estimated in linear regime from [7], [11] and in nonlinear regime using Eqs. (30)-(32) of Section IV, as was pointed out previously. In order to perform the estimation of these statistical parameters in both power regimes, the coupling coefficients k_{nm} and K_{nm} should be previously calculated. Using the fiber twisting rate f_T = 4 turns/m from the laboratory set-up and the fiber parameters of the multi-core fiber Fibercore SM-4C1500(8.0/125) with $n_n \approx 1.452$, $R_0 \approx 4$ μm, λ = 1550 nm and $d_{nm} \approx 35$ μm; $k_{nm} = 0.0072$ m^{-1} is obtained using Eq. 6(c) and K_{nm} is calculated from [12] for each bending radius as $K_{nm} = 5.13 \cdot 10^{-4}$ with $R_b = 67$ cm and $K_{nm} = 6.27 \cdot 10^{-4}$ with $R_b = 100$ cm.

As can be noted from Fig. 6, the theoretical estimations of the crosstalk statistical parameters fit correctly to the experimental measurements in linear and nonlinear regimes. The crosstalk mean in linear regime was estimated using Eq. (27) of [7] for R_b = 67 cm and Eq. (20) of [11] for R_b = 100 cm assuming a correlation length of the MCF structural fluctuations of $l_c \approx 4.9$ mm. As it was reported in [11], considering large bending radius (R_b = 100 cm), the linear crosstalk is induced by the structural fluctuations of the MCF as the major perturbation of core modes. In addition, the variance of the crosstalk and the number of phase-matching points in linear regime were estimated considering that both

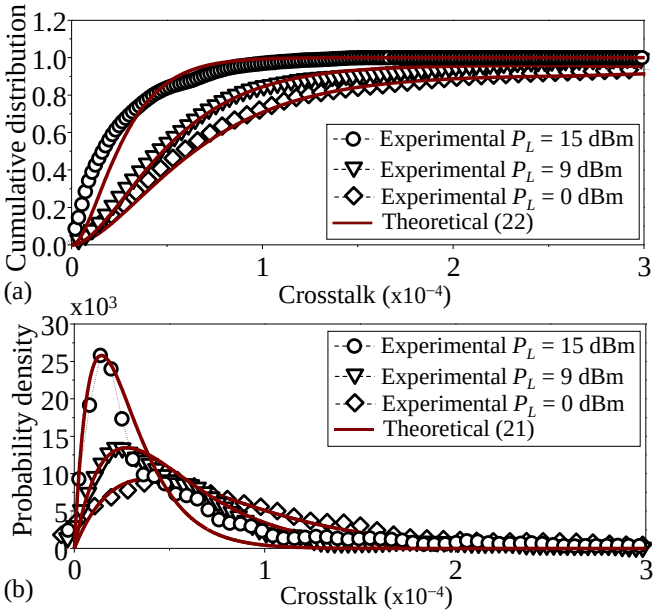

Fig. 7. Experimental results measured with R_b =100 cm for different optical power levels launched into core 3: (a) cumulative distribution function (cdf), and (b) probability density function (pdf). Circles: measured data for a power launch level of 15 dBm. Triangles: measured data for a power launch level of 9 dBm. Diamonds: measured data for a power launch level of 0 dBm.

parameters should satisfy the condition $\sigma^2_{L,nm} = (\mu_{L,nm})^2/2 = N_L^2 \cdot |K_{nm}|^4/2$, as was pointed out in Section IV. In nonlinear regime with $P_L \geq P_c$, the crosstalk mean ($\mu_{NL,nm}$), variance ($\sigma^2_{NL,nm}$) and the number of phase-matching points (N_{NL}) are in line with Eqs. (30)-(32) using b = 1/2, as confirmed in Fig. 6. Furthermore, it should be noted that the critical power P_c remains unchanged when varying the fiber bending radius.

The random nature of linear and nonlinear crosstalk was additionally investigated with the distribution functions given by Eqs. (21) and (22). Fig. 7 shows the measured evolution of the cdf and pdf of the crosstalk considering three different power launch levels P_L = 0, 9 and 15 dBm for a bending radius configuration of R_b = 100 cm. As verified in Fig. 7(a), the measured IC-XT cumulative distribution function satisfies the closed-form expression given by Eq. (22) for each power launch level. In addition, Fig. 7(b) shows the pdf evolution of the crosstalk with the power launch level injected into core 3 when using the same bending radius configuration. As we can notice, the measured IC-XT probability density function fits correctly to the chi-squared distribution with 4 d.f. given by Eq. (21). Due to the crosstalk mean and variance reduction in nonlinear regime, the higher the power launch level, the higher is the similitude of the cdf with the unit step function and the pdf with the Dirac delta function, as confirmed in Figs. 7(a) and (b) with P_L = 15 dBm.

On the other hand, the crosstalk distribution in multi-core excitation condition was experimentally evaluated injecting 0 dBm of optical power in three different cores using the laboratory set-up depicted in Fig. 8 with a bending radius configuration of R_b = 100 cm. The same ECL and EDFA of Fig. 5 were employed followed by three different 50/50 optical splitters with three VOAs to balance the optical power injected

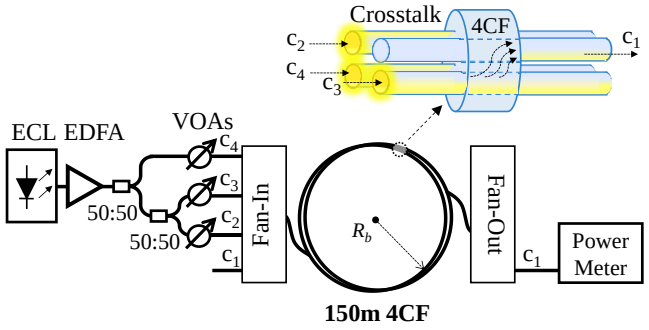

Fig. 8. Experimental set-up employed for crosstalk evaluation in multi-core excitation.

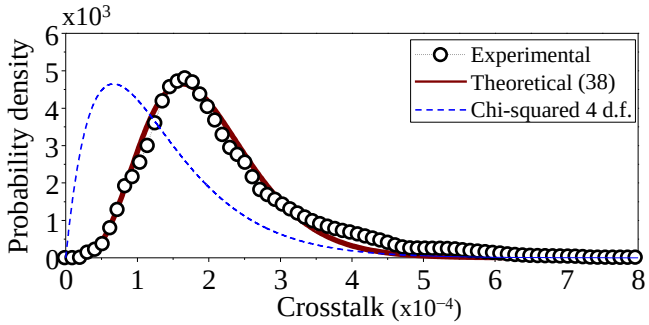

Fig. 9. Inter-core crosstalk (IC-XT) probability density function (pdf) analysis with multi-core excitation condition and R_b = 100 cm. IC-XT pdf measured from cores 2, 3 and 4 to core 1.

into cores 2, 3 and 4. The crosstalk pdf was measured in core 1 using the same method as in the single-core excitation. We previously verified that the splitting ratio of the optical splitters remained unchanged when sweeping the laser wavelength between 1550-1580 nm.

The crosstalk analysis in multi-core excitation condition should be performed considering only the excited adjacent cores. Therefore, stimulating cores 2, 3 and 4, the crosstalk in core 1 should be analyzed considering exclusively the mode coupling from cores 2 and 3. It can be noticed from Fig. 9 that the measured pdf of the crosstalk in core 1 fits correctly to Eq. (38) when using Eq. (21) to estimate the individual distributions $f_{X12}(y)$ and $f_{X13}(y)$ with N_L = 136 and 206, respectively. The crosstalk distribution $f_{X12}(y)$ was estimated from Eq. (21) with a lower number of phase-matching points than $f_{X13}(y)$ due to a slight difference in the crosstalk mean between these random process. Additionally, as it was pointed out in Section IV, the pdf of the crosstalk in multi-core excitation is identified with a chi-squared distribution higher than 4 d.f. due to the increment of the crosstalk variance induced by the convolution operation. A chi-squared distribution with 4 d.f. is inset in Fig. 9 for comparison. The crosstalk variance in core 1 is increased from $3.1\cdot10^{-9}$ to $5.7\cdot10^{-9}$ when cores 2, 3 and 4 are simultaneously excited.

Further investigation of the crosstalk in multi-core excitation will be evaluated in future works when all cores of the MCF are excited in nonlinear regime with the same optical power launch level. In this situation, it is expected that the Kerr effect will increase the refractive index of each core with the same value reducing the mismatching effect observed between the core modes.

VI. Conclusion

This paper reports the theoretical unification of linear and nonlinear inter-core crosstalk models in MCF media considering single-core and multi-core excitation. In order to estimate the crosstalk when a MCF is excited with high optical power levels, the coupled-mode and coupled-power theories were previously extended to nonlinear regime. The nonlinear coupled-mode theory was derived for both coupled and uncoupled MCF media. New mode-coupling coefficients were found and their closed-form expressions were proposed and analyzed for step-index single-mode MCFs varying the core pitch value and the index mismatching between cores. We verified that the dominant mode-coupling coefficients in linear and nonlinear regimes are k_{nm} and q_{1n}, respectively. However, the nonlinear cross-coupling effect given by q_{2nm} cannot be neglected in heterogeneous coupled MCFs with large index mismatching value Δn_{nm} and the core pitch lower than three times the core radius ($d_{nm} < 3R_0$). Considering these results, the coupled-power theory was also extended to nonlinear regime including the self-coupling power effect as the dominant nonlinear effect reducing the value of the equivalent power coupling coefficient $h_{nm,eq}$. Finally, the statistical model of the IC-XT was completed considering single-core and multi-core excitation. The closed-form expressions of the number of phase-matching points and the cumulative distribution function, probability density function, mean and variance of the nonlinear crosstalk were reported in single-core excitation conditions. In multi-core excitation, the crosstalk random process was identified as a chi-squared distribution with more than 4 degrees of freedom due to the convolution operation of the individual crosstalk distributions. The unified model was experimentally validated using a homogeneous 4CF with two different bending radius configurations confirming the suitability of the herein presented nonlinear analysis.

VII. Appendix
Derivation of Mode-Coupling Coefficients

The closed-form expressions of the mode-coupling coefficients (MCCs) given by Eqs. (6) are derived assuming step-index and single-mode cores with identical radius R_0, as was pointed out in Section II. It can be noticed from Eqs. (6) that the MCCs depend on the general term $\iint F_m^k F_n^s dS_\infty$, where $(k,s) \in \{0,1,2,3,4\}^2$. Using the analytic expression of [21] for the LP_{01} mode, the integral can be written in the cores and the cladding as follows:

$$\iint F_m^k F_n^s \mathrm{d}S_\infty = \int_r \int_\varphi \frac{K_0^k\left(\frac{w_m}{R_0}(r-d_{nm})\right)}{K_0^k(w_m)} \frac{J_0^s\left(\frac{u_n}{R_0}r\right)}{J_0^s(u_n)} \mathrm{d}S_n + \int_r \int_\varphi \frac{J_0^k\left(\frac{u_m}{R_0}(r-d_{nm})\right)}{J_0^k(u_m)} \frac{K_0^s\left(\frac{w_n}{R_0}r\right)}{K_0^s(w_n)} \mathrm{d}S_m + I_{cl}^{(k,s)} \quad (39)$$

where $I_{cl}^{(k,s)}$ describes the mode overlapping in the cladding.

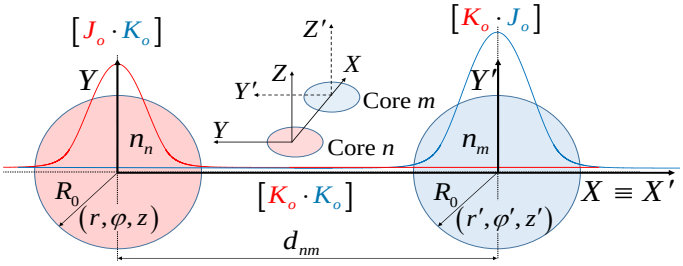

Fig. 10. Transversal functions F_n and F_m in the cross-sectional area of the heterogeneous TCF media.

Fig. 10 depicts the spatial distribution of the transversal function of the LP_{01} mode in the cross-sectional area of the TCF media. Note that the overlapping between the Bessel functions does not depend on the selected reference system satisfying the principle of general covariance. Therefore, the second term in the RHS of Eq. (39) can be calculated moving the reference system from core n with (r, ϕ, z) to core m with (r', ϕ', z'), as detailed in Fig. 10:

$$\iint_{r\ \varphi} \frac{J_0^k\left(\frac{u_m}{R_0}(r-d_{nm})\right)}{J_0^k(u_m)} \frac{K_0^s\left(\frac{w_n}{R_0}r\right)}{K_0^s(w_n)} \mathrm{d}S_m = \int_{r'=0}^{R_0}\int_{\varphi'=0}^{2\pi} \frac{J_0^k\left(\frac{u_m}{R_0}r'\right)}{J_0^k(u_m)} \frac{K_0^s\left(\frac{w_n}{R_0}(r'+d_{nm})\right)}{K_0^s(w_n)} r'\mathrm{d}r'\mathrm{d}\varphi' \quad (40)$$

Thus, assuming cores with identical radius R_0, Eq. (39) becomes:

$$\iint F_m^k F_n^s \mathrm{d}S_\infty \approx \approx 2\pi \left[\frac{K_0^k(w_m d_{nm}/R_0)}{K_0^k(w_m) J_0^s(u_n)} \int_0^{R_0} J_0^s\left(\frac{u_n}{R_0}r\right) r\mathrm{d}r + \frac{K_0^s(w_n d_{nm}/R_0)}{J_0^k(u_m) K_0^s(w_n)} \int_0^{R_0} J_0^k\left(\frac{u_m}{R_0}r'\right) r'\mathrm{d}r' \right] + I_{cl}^{(k,s)} \quad (41)$$

Similar to [23], the modified Bessel function of second kind K_0 has been approximated to its value in the center of the adjacent core due to the low slope of this function with $r, r' > R_0$. In addition, we can notice that the integrals in the RHS of Eq. (41) can be directly solved with $k,s \leq 2$ using [30]. Furthermore, with $k,s > 2$ the Gaussian approximation of J_0 function is employed with $r, r' < R_0$ [22] assuming an error lower than 1.5 % with J_0 function as reference:

$$J_0^{k(s)}\left(u_{n(m)} r / R_0\right) \approx \exp\left(-r^2 / H_{n(m)}^2\right)^{k(s)} \quad (42)$$

where $H_{n(m)}$ is given by Eq. (2.2.15) of [22]. Moreover, the denominator of Eqs. (6) is reduced to:

$$\iint F_n^2 \mathrm{d}S_\infty \approx \iint F_n^2 \mathrm{d}S_n = \frac{1}{J_0^2(u_n)} \int_0^{R_0}\int_0^{2\pi} J_0^2\left(\frac{u_n}{R_0}r\right) r\mathrm{d}r\mathrm{d}\varphi = \pi R_0^2 \left[1 + \frac{J_1^2(u_n)}{J_0^2(u_n)}\right] \quad (43)$$

where the approximation of Eq. (43) was performed considering the power of core n much higher than in the cladding with $\iint F_n^2 dS_n >> \iint F_n^2 dS_{clad}$.

From Eq. (21) of ref. [15], we found that the critical power of silica fibers required to stimulate the nonlinear polarization in the cores is around ~2dBm assuming an effective area of 80 μm^2. However, the power launch level required to stimulate the Kerr effect in the cladding should be increased around ~30 dBm assuming that the LP_{01} mode is highly confined in the cores [31]. Therefore, considering optical power launch levels lower than 30 dBm, we can assume that the third-order nonlinear polarization is not stimulated in the cladding. Thus, a silica MCF is equivalent to a MCF where the nonlinear nature is only restricted to the cores, with $\alpha_{NL}(\boldsymbol{r})$ coefficient null in the cladding. As a result, we can assume $I_{cl}^{(k,s)} \approx 0$ in the nonlinear mode-coupling coefficients q_{1n}, q_{2nm}, q_{3nm} and q_{4nm}, given by Eqs. (6d)-(6g). In addition, the Bessel function K_0^4 is neglected in q_{1n} coefficient Eq. (6d) considering that $\iint F_n^4 dS_n >> \iint F_n^4 dS_m$. On the other hand, taking into account that $\Delta\varepsilon_{rm}(\boldsymbol{r})$ and $\Delta\varepsilon_{rn}(\boldsymbol{r})$ are null in the cladding and in adjacent cores, as depicted in Fig. 1, the integrals in dS_∞ are restricted to dS_m and dS_n in c_n and k_{nm} coefficients, respectively. Finally, assuming weakly guiding approximation with $\beta_n \approx k_0 \cdot n_n$ and using Eqs. (41)-(43), the closed-form expressions of the linear and nonlinear MCCs Eqs. (6) are directly derived.

REFERENCES

[1] D. J. Richardson, et al., "Space-division multiplexing in optical fibres," *Nature Photon*., vol. 7, pp. 354−362, 2013.

[2] C. Antonelli, A. Mecozzi, and M. Shatif, "Scaling of inter-channel nonlinear interference noise and capacity with the number of strongly coupled modes in SDM systems," presented at the Optical Fiber Communication Conf. Exhibition, Anaheim, CA, USA, Mar. 2016, paper W4I.2.

[3] R.G.H. van Uden, R. A. Correa, E.A. López, F.M. Huijskens, C. Xia, G. Li, A. Schülzgen, H. de Waardt, A.M.J. Koonen, and C.M. Okonkwo, "Ultra-high-density spatial division multiplexing with a few-mode multi-core fibre," *Nature Photon.*, vol. 8, pp. 865-870, 2014.

[4] T. Mizuno, H. Takara, A. Sano, and Y. Miyamoto, "Dense space division multiplexed transmission over multi-core and multi-mode fiber," presented at the Optical Fiber Communication Conf. Exhibition, Los Angeles, CA, USA, Mar. 2015, Paper Th1D.2.

[5] P. J. Winzer, "High-spectral-efficiency optical modulation formats," *OSA/IEEE J. Lightw. Technol.*, vol. 30, no. 24, pp. 3824–3835, December 2012.

[6] R.-J. Essiambre, G. Kramer, P. J. Winzer, G. J. Foschini, and B. Goebel, "Capacity limits of optical fiber networks," *OSA/IEEE J. Lightw. Technol.*, vol. 28, no. 4, pp. 662–701, February 2010.

[7] T. Hayashi, T. Sasaki, E. Sasaoka, K. Saitoh, and M. Koshiba, "Physical interpretation of intercore crosstalk in multicore fiber: effects of macrobend, structure fluctuation, and microbend," *OSA Opt. Exp*., vol. 21, no. 5, pp. 5401–5412, February 2013.

[8] R. S. Luis et al., "Experimental Evaluation of the Time and Frequency Crosstalk Dependency in a 7-Core Multi-Core Fiber," presented at the Optical Fiber Communication Conf. Exhibition, Los Angeles, CA, USA, Mar. 2015, paper W4I.3.

[9] M. Koshiba, K. Saitoh, K. Takenaga, and S. Matsuo, "Multi-core fiber design and analysis: coupled-mode theory and coupled-power theory," *OSA Opt. Exp*., vol. 19, no. 26, pp. B102–B111, November 2011.

[10] T. Hayashi, "Multi-core Optical Fibers," in *Optical Fiber Telecommunications VIA: Components and Subsystems*, I. P. Kaminow, T. Li, and A. E. Willner, Eds., New York: Elsevier, 2013, ch. 9.

[11] M. Koshiba, K. Saitoh, K. Takenaga, and S. Matsuo, "Analytical expression of average power-coupling coefficients for estimating

intercore crosstalk in multicore fibers," *IEEE Photon. Journal*, vol. 4, no. 5, pp. 1987–1995, October 2012.
[12] T. Hayashi, T. Taru, O. Shimakawa, T. Sasaki, E. Sasaoka, "Design and fabrication of ultra-low crosstalk and low-loss multi-core fiber," *OSA Opt. Exp*., vol. 19, no. 17, pp. 16576–16592, August 2011.
[13] S. Mumtaz, R.-J. Essiambre and G. P. Agrawal, "Reduction of Nonlinear Penalties Due to Linear Coupling in Multicore Optical Fibers," *IEEE Photon. Techn. Lett.*, vol. 24, no. 18, pp. 1574–1576, September 2012.
[14] S. Mumtaz, R.-J. Essiambre and G. P. Agrawal, "Nonlinear Propagation in Multimode and Multicore Fibers: Generalization of the Manakov Equations," *OSA/IEEE J. Lightw. Technol.*, vol. 31, no. 3, pp. 398–406, February 2013.
[15] A. Macho, M. Morant, and R. Llorente, "Experimental evaluation of nonlinear crosstalk in multi-core fiber," *OSA Opt. Exp*., vol. 23, no. 14, pp. 18712–18720, July 2015.
[16] S. Ö. Arik and J. M. Kahn, "Coupled-core multi-core fibers for spatial multiplexing," *IEEE Photon. Techn. Lett.*, vol. 25, no. 21, pp. 2054–2057, November 2013.
[17] T. Sakamoto, T. Mori, M. Wada, T. Yamamoto, and F. Yamamoto, "Coupled multicore fiber design with low intercore differential mode delay for high-density space division multiplexing," *OSA/IEEE J. Lightw. Technol.*, vol. 33, no. 6, pp. 1175–1180, March 2015.
[18] S. M. Jensen, "The nonlinear coherent coupler," *IEEE Trans. Microwave Theory and Techniques*, vol. 30, no. 10, pp. 1568–1571, October 1982.
[19] F. J. Fraile-Pelaez and G. Assanto, "Coupled-mode equations for nonlinear directional couplers," *OSA Applied Optics*, vol. 29, no. 15, pp. 2216–2217, May 1990.
[20] W.-P. Huang, "Coupled-mode theory for optical waveguides: an overview," *J. Opt. Soc. Am*. vol. 11, no. 3, 963–983, pp. March 1994.
[21] D. Gloge, "Weakly guiding fibers," *OSA Applied Optics*, vol. 10, no. 10, pp. 2252–2258, October 1971.
[22] G. P. Agrawal, *Nonlinear Fiber Optics*, 5th ed. San Diego, CA: Academic Press, 2013, ch. 2.
[23] A. W. Snyder, "Coupled-mode theory for optical fibers," *J. Opt. Soc. Am*. vol. 62, no. 11, pp. 1267–1277, November 1972.
[24] K. Okamoto, *Fundamentals of Optical Waveguides*, Elsevier, 2006, ch. 4.
[25] M. Morant, A. Macho, and R. Llorente, "On the suitability of multicore fiber for LTE-advanced MIMO optical fronthaul systems," *OSA/IEEE J. Lightw. Technol.*, vol. 34, no 2, pp. 1-7, 2016.
[26] D. Marcuse, *Theory of Dielectric Optical Waveguides*, Elsevier, 1974, ch. 5.
[27] M. Koshiba, "Design aspects of multicore optical fibers for high-capacity long-haul transmission," presented at the IEEE International Topical Meeting on Microwave Photon. and the Asia-Pacific Microwave Photon. Conf., pp. 318–323, October 2014.
[28] H. P. Hsu, *Probability, Random Variables, & Random Processes*, McGraw-Hill, 1997, ch. 4–6.
[29] T. Hayashi, T. Taru, O. Shimakawa, T. Sasaki, and E. Sasaoka, "Characterization of crosstalk in ultra-low-crosstalk multi-core fiber," *OSA/IEEE J. Lightw. Technol.*, vol. 30, no. 4, pp. 583–589, February 2012.
[30] A. W. Snyder and J. D. Love, *Optical Waveguide Theory*, Chapman & Hall, 1983, ch. 37.
[31] Y. Guo, C. K. Kao, E. H. Li, and K. S. Chiang, *Nonlinear Photonics, Nonlinearities in Optics, Optoelectronics and Fiber Communications*, Springer, 2002, ch. 9.

Andrés Macho (S'14) received the Telecommunication Engineering degree (M.Sc.) from the ETSIT-Universidad Politécnica de Madrid in 2013. He worked in 2014 at Telefonica R&D Corporation in the Core Network Evolution group and he collaborated in some R&D European projects such as FP7-STRAUSS, FP7-DISCUS and H2020-INSPACE.

Currently, he is working towards the Ph.D. degree at Valencia Nanophotonics Technology Center at the Universitat Politècnica de València. His professional interest includes high-capacity wavelength-division multiplexed networks (WDM), modal analysis of multi-core fibers, advanced optical modulation formats and space-division multiplexing optical transmissions.

Maria Morant (S'07-M'12) received the M.Sc. degree in Telecommunication Engineering in 2008 and obtained the International Ph.D. degree from the Universitat Politècnica de València, Spain, in 2012. Since 2006, she has investigated optical techniques for the transmission of OFDM-based signals in access networks at Valencia Nanophotonics Technology Center (NTC).

She is currently a post-doc researcher at NTC leading the research project OESED "Optically enhanced spectral coherent detection" dealing with advanced optical sensing. She has participated in European projects dealing with optical communications and optical sensing such as FP7-ICT-FIVER, FP7-IST-UCELLS and FP6-IST-UROOF and in national projects like ULTRADEF, VISICONEC and HIDRASENSE. She has contributed with more than 75 papers to international journals and hot-topic conferences on optical communications. Her current research areas of interest include advanced modulations and optical sensing techniques.

Roberto Llorente (S'99-S'06), M.Sc. degree in Telecommunication Engineering from the Universitat Politècnica de València (UPV), Spain, received the European Ph.D. degree from the same University in 2006. Since then, he has been in research positions within the university, and in 2002 he joined the Valencia Nanophotonics Technology Center (NTC) as research associate.

Currently, he is professor in the UPV teaching Optical Communications-related subjects. He is also Head of the Optical Systems and Networks Unit in the NTC. He has been leading NTC activities in the European projects FP5-IST-TOPRATE and FP6-ISTUROOF between others. He has proposed and coordinated FP7-IST-UCELLS and FP7-ICT-FIVER projects in the field of radio-over-fibre technology and next-generation FTTH networks. Currently, he is leading NTC activities in national and international research projects dealing with optical signal processing applied to optical networks and next-generation test & measurement.

He has authored or co-authored more than 150 papers in leading international journals and conferences and has authored three patents. His current research interest includes optical and electro-optical processing applied to optical core and metro networks, hybrid wireless-optical access networks, optical sensing, metrology, and medical imaging systems.